Journal of Molecular Graphics and Modelling 39 (2013) 183–192

Contents lists available at SciVerse ScienceDirect

Journal of Molecular Graphics and Modelling

journal homepage: www.elsevier.com/locate/JMGM

Replica exchange molecular dynamics simulation of chitosan for drug delivery system based on carbon nanotube

Chompoonut Rungnim[a], Thanyada Rungrotmongkol[b], Supot Hannongbua[c,*], Hisashi Okumura[d,e]

[a] Nanoscience and Technology Program, Graduate School, Chulalongkorn University, Bangkok 10330, Thailand
[b] Department of Biochemistry, Faculty of Science, Chulalongkorn University, Bangkok 10330, Thailand
[c] Computational Chemistry Unit Cell, Department of Chemistry, Faculty of Science, Chulalongkorn University, Bangkok 10330, Thailand
[d] Research Center for Computational Science, Institute for Molecular Science, Okazaki, Aichi 444-8585, Japan
[e] Department of Structural Molecular Science, The Graduate University for Advanced Studies, Okazaki, Aichi 444-8585, Japan

ARTICLE INFO

Article history:
Received 6 June 2012
Received in revised form 29 October 2012
Accepted 3 November 2012
Available online 6 December 2012

Keywords:
Replica exchange molecular dynamics simulation
Targeted drug delivery system
Carbon nanotube
Chitosan
Gemcitabine
Implicit solvation model

ABSTRACT

Chitosan is an important biopolymer in the medical applications because of its excellent biocompatibility. It has been recently highlighted in the targeted drug delivery system (DDS) by improvement of the carbon nanotube (CNT) solubility. To investigate the effect of chitosan length, the two targeted DDSs with 30 and 60 chitosan monomers were performed by replica-exchange molecular dynamics simulations at temperatures in the range of 300–455 K with three different combinations of force fields and implicit solvation models. Each DDS model contains the epidermal growth factor (EGF), chitosan (CS) of 30 (30CS) and 60 (60CS) monomers, single-wall CNT (SWCNT) and gemcitabine (Gemzar) as the model payload anticancer drug, called EGF/30CS/SWCNT/Gemzar and EGF/60CS/SWCNT/Gemzar, respectively. The SWCNT confines gemcitabine inside its cavity, while the outer surface is wrapped by chitosan in which one end is linked to the EGF. Even though the REMD results from different force fields and implicit solvation models are not exactly identical, all of them are in the same trend confirming that in the EGF/30CS/SWCNT/Gemzar DDS the 30CS chain was not long enough to wrap around the SWCNT, and consequently the EGF was located so close to the tube as to potentially cause steric inhibition of the binding of EGF to its receptor (EGFR), which is highly expressed on the surface of cancer cells. On the other hand, this phenomenon is not observed in the EGF/60CS/SWCNT/Gemzar DDS in which the 60CS was found to completely wrap over the CNT outer surface using only 50 chitosan units. The evidence suggested that a ratio of chitosan molecular weight per SWCNT surface area larger than 9.9×10^{-7} kg/m^2 is suitable for application in targeted DDSs. Although an increase in the temperature is likely to influence the overall DDS structure, and especially the orbit of helical chitosan on the SWCNT and the EGF conformation, gemcitabine is still encapsulated inside the tube.

1. Introduction

Single walled carbon nanotubes (SWCNTs) [1] are known as a smart material for specific targeted drug delivery systems (DDSs) because of their unique size, shape and ability to functionalize with other molecules, e.g., drugs, biopolymers and proteins [2–5]. However, the low dispersion of pristine SWCNTs in aqueous solution is a typical drawback of its applications [6]. To overcome the problem, the outer surface is modified by the covalent functionalization with charged molecules or is non-covalent functionalized with biopolymers, such as alginate and chitosan [7–9]. For instance, the molecular dynamics (MD) simulations [10] revealed that chitosan wrapped around SWCNTs can significantly increase their dispersion and solubility. Furthermore, the *in vitro* pH-triggered drug loading and release from SWCNTs modified by chitosan has been successfully demonstrated [11]. The ability of chitosan to conjugate with other biomolecules offers the opportunity to use it as a polymer for drug carriers in many DDS applications [12–15].

According to the data from World Health Organization (WHO) [16], the diverse group of ailments collectively known as cancer is a leading cause of death worldwide, with millions of patients around the world suffering from one form or another of cancer. Despite the diversity of cancers, many appear to share conserved attributes at the molecular level making these clear targets for treatment. However, the severe side effects of current broad systemic cancer therapies, especially chemotherapy, have driven extensive research toward finding the best way to treat the patients with

* Corresponding author at: Computational Chemistry Unit Cell, Department of Chemistry, Faculty of Science, Chulalongkorn University, Bangkok 10330, Thailand.
E-mail address: supot.h@chula.ac.th (S. Hannongbua).

1093-3263/$ – see front matter © 2012 Elsevier Inc. All rights reserved.
http://dx.doi.org/10.1016/j.jmgm.2012.11.004

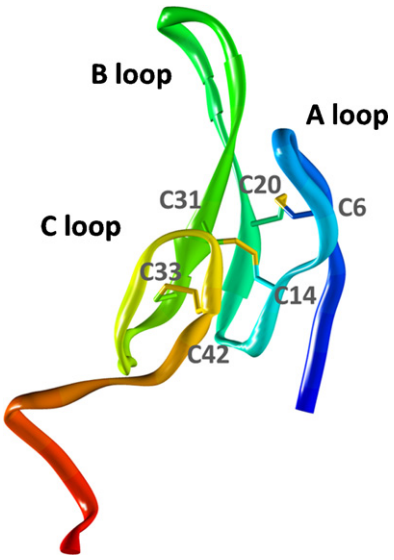

Fig. 1. Schematic view of EGF showing the three loop domains (A–C) and the three internal cysteine linkages.

current anticancer drugs, and especially for targeted delivery, as well as for new drug development. Specific cancer cell (or at least tissue) targeted DDSs are currently one of the most promising candidates because they can be designed to give precise delivery of an effective dose of the anticancer drug to the tumor cells with high specificity without the need for both systemic uptake following administration, eliminating the side effects to normal cell areas, and the oscillation cycles between overdoses to underdoses, again reducing the systemic toxic side effects to normal proliferating tissues [17,18]. The growth and cell division rate of cancer cells are remarkably fast and faster than most normal cells, and so, as expected, cancer cells typically express elevated levels of key growth factor receptors, such as the folic acid receptor and epidermal growth factor (EGF) receptor (EGFR) [19–21]. Therefore, ligands (typically the natural ones) with a high affinity to these receptors are used as specific targeting agents in DDSs for cancer treatment, including folic acid and EGF [22–25].

EGF is a small protein with only 53 amino acids, and consists of three distinct loops, A: C6–V19, B: C20–C31 and C: C33–C42, which are divided by three disulfide bridges, C6–C20, C14–C31 and C33–C42 [26,27], as shown schematically in Fig. 1.

The two-stranded antiparallel β-sheet of the B loop has been found to be the major structural element of EGF and is an important region in binding to the EGFR [28]. The binding of EGF to the EGFR (HER1 or ErbB1, a member of the ErbB family) induces EGFR dimerization, which then activates specific tyrosine kinase signaling at the intracellular region of the EGFR, and, importantly, internalization of the dimeric EGFR–ligand complex [29–31], enabling the use of EGF as a targeting molecule for DDSs. EGFR is a family of transmembrane proteins that act as receptors for multiple ligands (including EGF and TGFα) involved in cell growth processes, such as proliferation, transformation and deviation, by controlling the communication between the components outside and the inside the cells [32,33].

EGFR has been found to be over-expressed in many types of epithelial cell cancers, such as lung [34,35], breast [36], ovarian and cervical cancers [37], and indeed mutations in the EGFRs that lead to over expression are found in some 30% of all epithelial cancers. Therefore, the attachment of EGF to SWCNT could increase the specificity of SWCNT-based DDSs to such cancer cells. For example, Bhirde et al. [38] discovered that SWCNTs directly conjugated on their outer surface to EGF via the carboxylic functional group were able to deliver anticancer drugs *in vivo* to cancer cells with a high degree of selectivity. The chitosan decorated on the SWCNT surface was also used to link with other relatively specific cancer cell targeting agents, such as folic acid [15,39]. Besides the increase in the specificity of SWCNT-based DDSs, it also provides the advantage of potential thermal ablation based cancer therapy. Here, the targeted SWCNTs can be utilized to trigger the release of encapsulated molecules or even specifically destroy the tumor cells via near-infrared (NIR) treatment [40,41]. However, the molecular information of the specific targeted DDSs under various temperatures, which is important to allow the development of more effective DDS has not been demonstrated.

Gemcitabine, trade named as Gemzar, is a 2′ Fluoro-nucleoside analog of deoxycytidine that, along with other nucleoside analogs like fluorouracil, inhibits DNA replication via blocking deoxynucleotide (in this case cytidine) incorporation into DNA strand synthesis and also inhibiting ribonuclease reductase activity, so preventing DNA replication and repair leading to cell death. Thus, it is active against all dividing cells, as well as those undergoing DNA repair, and so shows adverse side effects when sued for chemotherapy against cancer. Thus, it was selected as a suitable representative model drug for targeted delivery.

MD simulations have been used for more than 50 years to help understanding physical phenomena at a molecular scale in numerous complex systems in many fields, including material science, nanotechnology and biology [42–46]. Investigations on biomolecule and drug behaviors in DDS applications have been performed using MD simulations [47–49]. Since most MD simulation studies are based on canonical ensemble simulations, the presence of many local minima traps that cause a limited range of sampling and sometimes lead to incorrect results is potentially a serious problem. Increasing the simulation temperature can enhance the probability to cross the barrier from one minimum to another with the consequence of a higher probability of attaining the global minimum. Replica-exchange molecular dynamics (REMD) simulations try to solve this problem by exchanging non-interacting replicas of the system at several temperatures [50–55]. Nowadays, this approach has been used to not only modify REMD to investigate protein conformations, but also to apply the method to explore the effect of temperature on the denaturation of proteins [56–61]. Up to date, most of REMD studies likely use implicit solvation model to reduce computation resource in calculation of water molecular interactions by incorporating properties of solvent into energy function and neglecting the geometry as well as details of solvent hydrogen bond patterns [62]. One of the common implicit solvation models called generalized born (GB) model [63] gives an appropriate results in good agreement with explicit solvation. However, accuracy of calculations using the implicit solvation model is depended on either solvation model or force field applied. For example, Shell et al. [64] studied effect of AMBER force fields with different GB solvation models, igb1 from Hawkins, Cramer and Truhlar (HCT) [65], igb5 from Onufriev, Bashford and Case (OBC) [66,67], and igb7 from Mongan et al. [68], on the secondary structure of proteins. From REMD simulations, they found that AMBER96 force field with igb5 solvation model (ff96/igb5) was a good combination to preserve the protein structure with a balance between strand and helical conformations. Besides, ff03/igb5 and ff96/igb1 were also reported to give consistent results in their study.

Herein, the REMD simulations with ff96/igb1, ff96/igb5 and ff03/igb5 were applied on the two studied systems, SWCNT-based DDSs with different chitosan lengths, 30 (30CS) or 60 (60CS) units, wrapped on the SWCNT. Each system contains the SWCNT drug transporter, EGF specific targeting agent, chitosan surface modification for the SWCNT as well as acting as a linker to attach the EGF to the SWCNT, and gemcitabine as the model payload anticancer drug. The structure properties and orientations of each DDS component under REMDs using different force fields and implicit

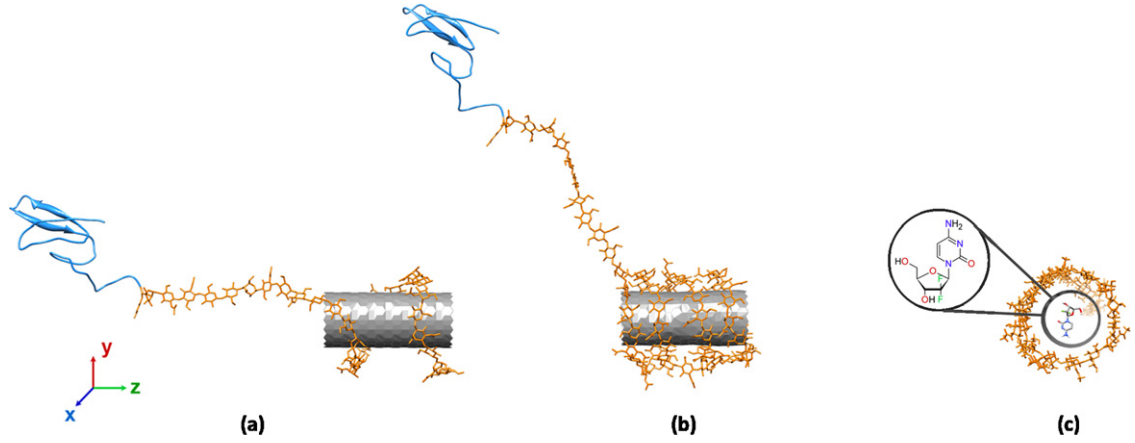

Fig. 2. Schematic view of the initial DDS structure of (a) the EGF/30CS/SWCNT/Gemzar and (b) the EGF/60CS/SWCNT/Gemzar DDSs. EGF is represented as a blue ribbon and the chitosan units are shown as an orange line wrapped around the SWCNT (gray surface). Gemcitabine is located inside the SWCNT cavity as seen in (c) the cross-section view of the SWCNT. (For interpretation of the references to color in this figure legend, the reader is referred to the web version of the article.)

solvation models were extensively discussed. The influence of chitosan length (30CS or 60CS) to the structure and conformation of the two DDS models was compared. Moreover, the effect of temperature to all the components, EGF, chitosan and encapsulated gemcitabine, were explored in terms of molecular behavior and conformation.

2. Computational methods

2.1. System preparation

The molecular structures of the two DDSs in this study were composed of four components; SWCNT, EGF, chitosan of two different chain lengths (30CS and 60CS) and gemcitabine (Gemzar) as the model payload anticancer drug to form the two DDSs termed as EGF/30CS/SWCNT/Gemzar and EGF/60CS/SWCNT/Gemzar, respectively. The structure of EGF and gemcitabine were obtained from the protein databank as PDB entry codes INQL [31] and 2NO0 [69], respectively. The 30CS and 60CS monomers were helically wrapped on (18,0) zig–zag SWCNT with 14 Å in diameter and 34 Å in length using the Material Studio 4.3 package software. Both the 30CS and 60CS chains had a 60% degree of deacetylation (%DD) in a random sequence of N-acetyl-D-glucosamine (NAG) and D-glucosamine (GLS) monomers. The 60% DD level was chosen because it is reported to be the lowest %DD that significantly improved dispersion of SWCNTs [7]. The chitosan chain in the EGF/30CS/SWCNT/Gemzar DDS contained 12 NAG and 18 GLS, whilst the EGF/60CS/SWCNT/Gemzar DDS contained 24 NAG and 36 GLS units. To construct the complex system, EGF was covalently linked to the chitosan chain via a peptide bond between the backbone carbonyl carbon of R53 at the C terminal end of EGF and the nitrogen of the first chitosan unit. The gemcitabine, used as a model anticancer drug, was located inside the center of the SWCNT cavity, as shown schematically in Fig. 2c. The initial structures of the two systems are depicted in Fig. 2a and b.

The molecular topologies of the EGF/30CS/SWCNT/Gemzar and EGF/60CS/SWCNT/Gemzar systems were created according to the standard procedures using the antechamber program in the AMBER10 software [63,70,71]. The parameters of EGF and SWCNT were modeled using the AMBER03 force field [72], while the GLYCAM06 force field [73] was applied for chitosan. The partial charges and parameters of gemcitabine were as previously reported [74]. To investigate the effect of implicit solvation model, three sets of combination between AMBER force fields and GB implicit solvation models, ff96/igb1, ff96/igb5 and ff03/igb5, were applied on the EGF/30CS/SWCNT/Gemzar and EGF/60CS/SWCNT/Gemzar DDSs with total number atoms of 2186 and 2906, respectively.

2.2. Replica exchange molecular dynamics (REMD) simulation

All calculations for the EGF/30CS/SWCNT/Gemzar and EGF/60CS/SWCNT/Gemzar DDSs REMD simulations with different pairs of AMBER force fields and implicit solvation models (ff96/igb1, ff96/igb5 and ff03/igb5) were performed using the AMBER10 software package. First of all, the complexes were minimized with 2500 steps of steepest descent. The minimized structures were subsequently subjected to REMD simulations over a temperature range of 300–455 K. Note that one advantage of CNT as a drug carrier for targeted DDS is the use of thermal abrasion cancer therapy to raise the temperature of CNT to be over 100 °C using 390-mW/1064 nm laser [75], therefore, this temperature range (300–455 K) was chosen in the present study. The average acceptance ratio was adjusted in the range of 20–50% probability by setting the number of replicas to 32 with the difference in the temperature between each replica being 5 K. Afterwards, equilibration of overall structure at each temperature was performed for 20 ps. The final structure at each temperature was used as the starting conformation for REMD simulation. The replica exchanges were attempted every 1 ps and each replica was simulated for 5 ns. During the simulations, the trajectory frames were recorded every 2 ps. After the simulation ends, the trajectories after 2.5 ns were used for all analyses.

3. Results and discussion

3.1. Energy surfaces

The 2D free-energy landscapes at the lowest temperature, 300 K, of the EGF/30CS/SWCNT/Gemzar and EGF/60CS/SWCNT/Gemzar systems are illustrated in Fig. 3a and b, respectively. The free-energies were calculated as a function of two order parameters, $F(x, y)$, as shown in Eq. (1):

$$F(x, y) = -k_B T \log[P(x, y)] \quad (1)$$

where x is the distance between the centers of gravity of EGF and CNT, d[Cg(EGF) – Cg(CNT)], while y is the distance between the centers of gravity of the first and the last chitosan units for EGF/30CS/SWCNT/Gemzar and EGF/60CS/SWCNT/Gemzar, d[Cg(^{1st}CS) – Cg(^{30th}CS)], and d[Cg(^{1st}CS) – Cg(^{60th}CS)]

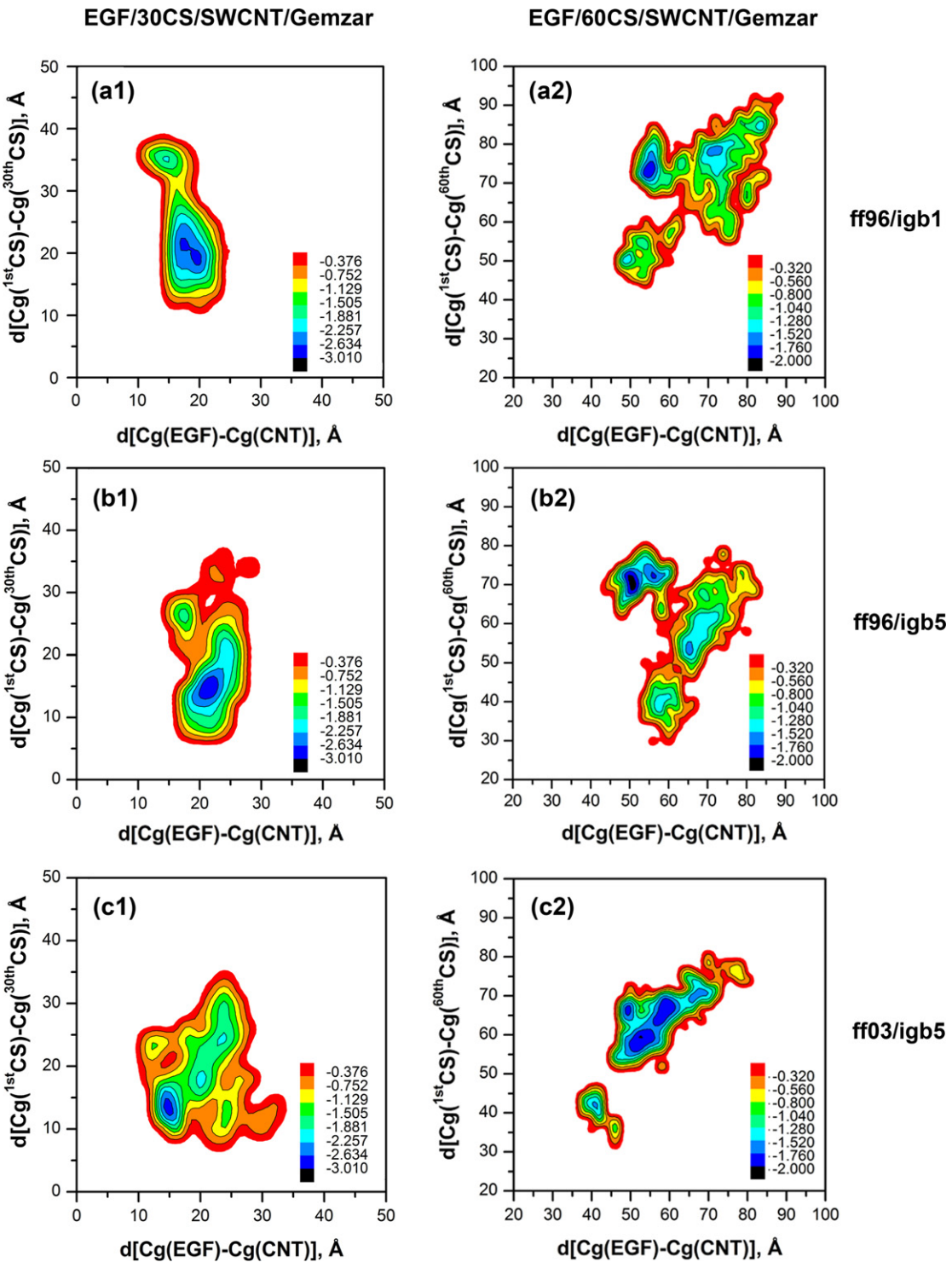

Fig. 3. The 2D free-energy surface of the EGF/30CS/SWCNT/Gemzar and EGF/60CS/SWCNT/Gemzar DDSs at 300 K from REMD simulations with ff96/igb1, ff96/igb5 and ff03/igb5.

respectively. Boltzmann constant is k_B while T is the temperature (K) and $P(x, y)$ is the probability of x, y parameters distribution.

For the EGF/30CS/SWCNT/Gemzar DDS, the potential energy surfaces calculated from REMD simulations with ff96/igb1 and ff96/igb5 shown in Fig. 3a1 and b1 are nearly in the same pattern: (i) the global minimum with the highest probability of finding located in a range of (17–21 Å, 18–22 Å) and (19–23 Å, 13–17 Å) and (ii) the local minimum with the secondary probability of finding at (14–15 Å, 35–36 Å) and (17–18 Å, 25–28 Å). Meanwhile, the global minimum from ff03/igb5 result is positioned at (13–16 Å, 12–15 Å) with the four noticeable local minima (Fig. 3c1). Interestingly, all three simulations indicated that 30CS chain enfolded tightly around the SWCNT pulling the EGF closer to center of the SWCNT as shown in Fig. 4a1–c1. Although the distance between the two chitosan ends, $d[Cg(^{1st}CS) - Cg(^{30th}CS)]$, at initial state was 79 Å, the length dramatically shortened to be <25 Å in all global minimum structures which is significantly less than the SWCNT length (34 Å). This implies that the 30 chitosan units were

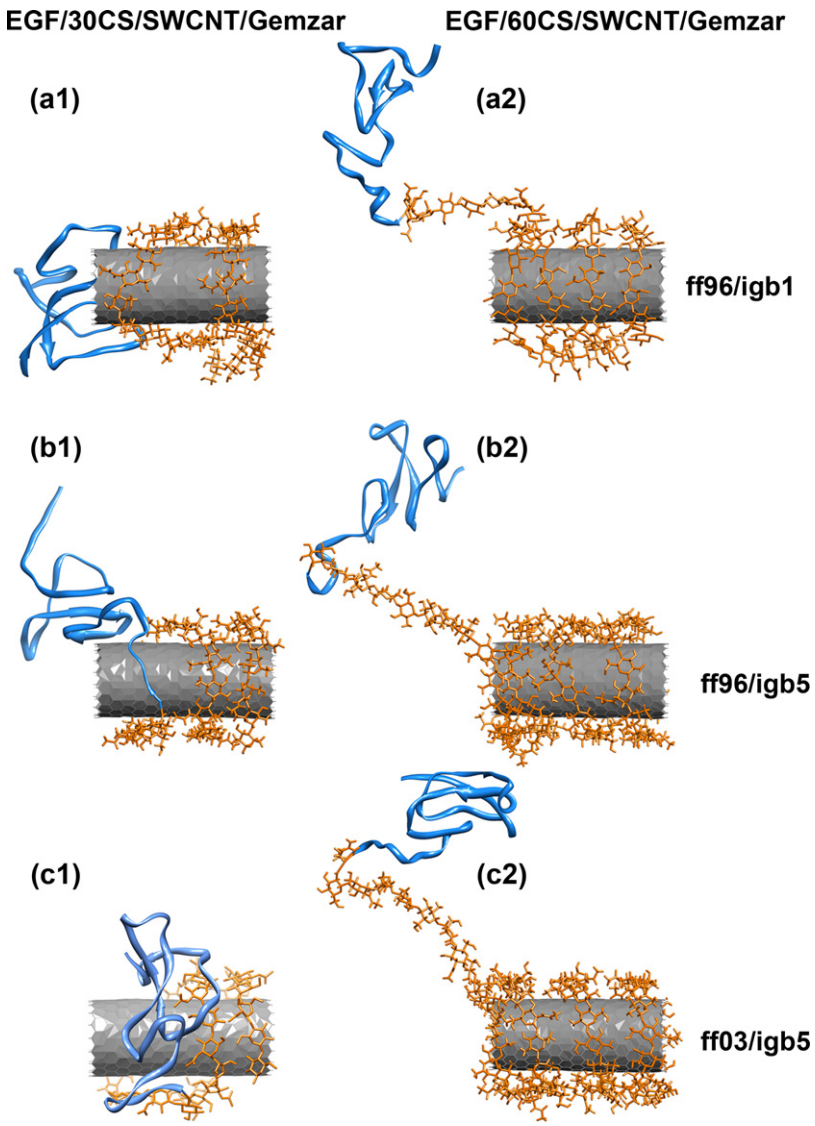

Fig. 4. Representative schematic view for the global minimum structure of each REMD simulations with ff96/igb1, ff96/igb5 and ff03/igb5.

insufficient to cover the entire surface of the studied tube. On the other hands, the shortened *d*[Cg(EGF) – Cg(CNT)] at the global minimum structure referred that the EGF was forced to locate closer to the tube due to the tightly enfolded 30CS chain.

At the initial structure of EGF/60CS/SWCNT/Gemzar DDS, the *d*[Cg(EGF) – Cg(CNT)] was 91 Å while the *d*[Cg(^{1st}CS) – Cg(^{60th}CS)] was 85 Å. Although the energy surface for the three simulations are likely different, the structure at global minimum obtained from the simulations with ff96/igb1 and ff96/igb5 was located nearly the same location at (53–56 Å, 71–75 Å in Fig. 3a2) and (50–52 Å, 69–73 Å in Fig. 3b2). In case of the simulation with ff03/igb5 (Fig. 3c2), the global minimum structure was placed at decreased *d*[Cg(^{1st}CS) – Cg(^{60th}CS)] of 55–62 Å while the *d*[Cg(EGF) – Cg(CNT)] was almost equal to that of the previous two systems (50–56 Å). It is a worth to note that the *d*[Cg(^{1st}CS) – Cg(^{60th}CS)] of all global minimum structures was dramatically longer than the SWCNT length (34 Å), and thus it was completely wrapped over the tube surface (Fig. 4a2–c2). In addition, the *d*[Cg(EGF) – Cg(CNT)] values of all simulated structures of the 60CS system (38–85 Å, Fig. 3a2–c2) were higher than a half tube length (17 Å) suggesting that EGF did not lay on tube surface (Fig. 4a2–c2) in contrast to those of the 30CS system (10–33 Å, Figs. 3a1–c1 and 4a1–c1).

3.2. EGF

The basic information on temperature dependence of the DDS components, i.e., EGF, chitosan and gemcitabine drug, can be revealed by REMD simulation. To investigate the EGF conformation in the DDS models, the protein secondary structures were analyzed using the DSSP algorithm [76] and summarized in Fig. 5 with β-sheet formational probability of each residue. Note that the β-sheet in the B-loop of EGF (Fig. 1) is significant for binding with EGFR [28]. In according to the EGF crystal structure, the major β-sheet formation locate at the residues V19–I23 and K28–N32, while the others take place nearby the N terminal (S4–E5 and Y13–C14) and C terminal (Y37–I38 and Y44–R45).

From the secondary structure analysis of EGF/30CS/SWCNT/Gemzar DDS (Fig. 5a1–c1), in the simulations using igb5 solvation model the V19–I23 and K28–N32 showed a β-sheet formation (red) with probability of 0.7 (black in Fig. 5b3 and c3), while this probability was dramatically reduced to 0.3 in the igb1 simulation (Fig. 5a3) suggesting the deformation of the secondary structure at these residues (Fig. 5a1). For the β-sheet at the N terminal end, the disappearance of β-sheet formation was found due to the high flexible N terminus in the ff96 simulations but was changed its conformation to be helix structure in the ff03

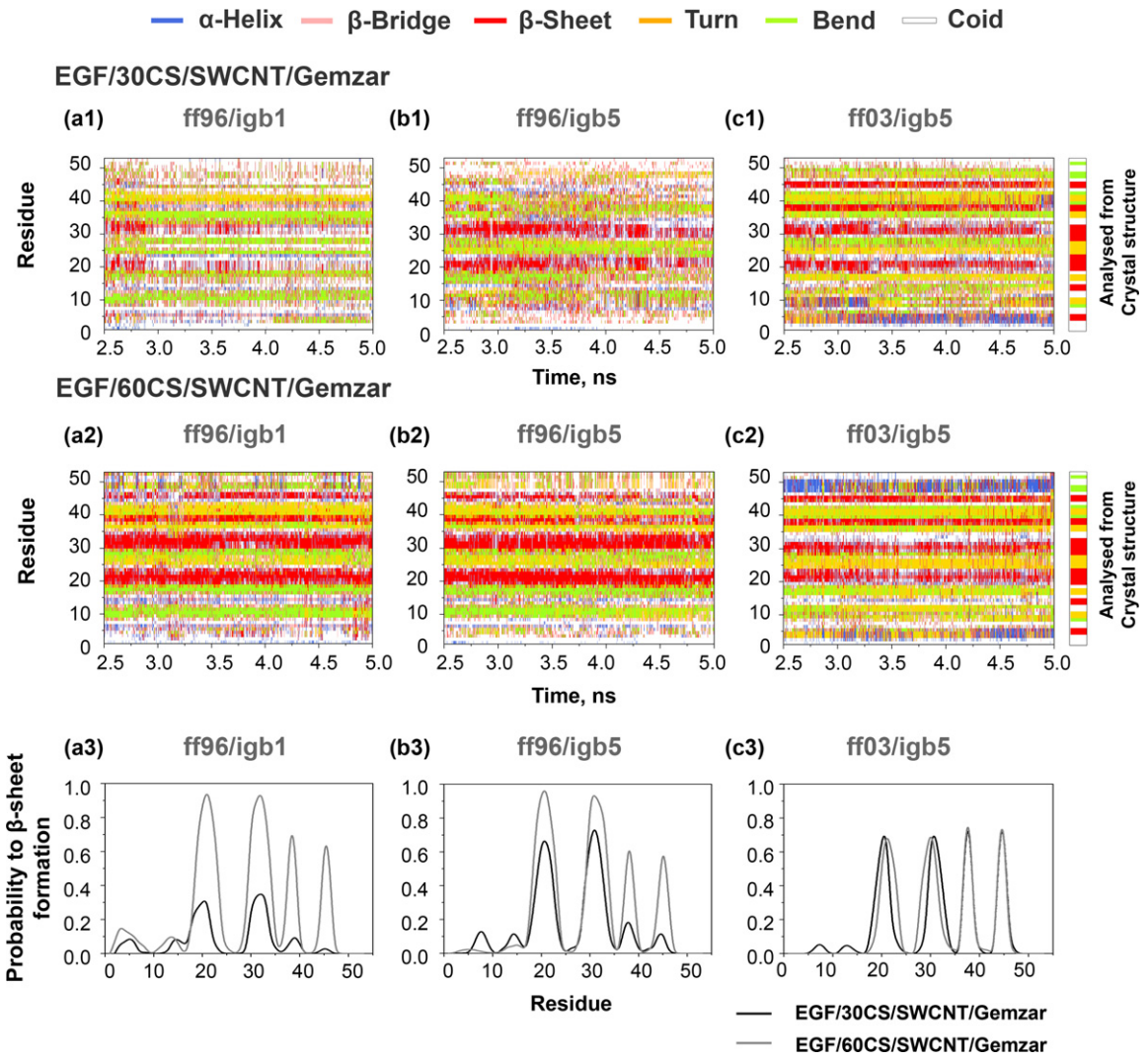

Fig. 5. Secondary structure analysis of EGF at 300 K obtained from three simulations sets of EGF/30CS/SWCNT/Gemzar and EGF/60CS/SWCNT/Gemzar DDS with the probability to form β-sheet conformation of each EGF residue.

simulation. In case of the β-sheet at the C terminus with which the first unit of chitosan chain was covalently linked, the simulation with ff03/igb5 provides the probability of 0.7 but <0.2 in the rest two simulations indicating the appearance and disappearance of β-sheet formation, respectively. In the EGF/60CS/SWCNT/Gemzar DDS, the major β-sheet was remarkably found in all three simulations (red in Fig. 5a2–c2) with the probabilities of 0.9 and 0.7 for the ff96 and ff03 simulations, respectively (gray in Fig. 5a3–c3). The β-sheet formation near to N terminus was not observed but that of another end was formed in all simulations with average probability of 0.7 (gray in Fig. 5a3–c3). Taken together, the major β-sheet conformation of EGF was better preserved in the 60CS system than that of the system with the shorter chitosan chain. The dramatically structural change in the EGF β-sheet of the 30CS system may lead to a disappropriate binding to its receptor, EGFR.

To determine such specific binding of EGF from the studied DDS models toward its receptor EGFR, EGF in the representative global minimum structure from the ff03/igb5 simulations (Fig. 4c1 and c2 for the 30CS and 60CS systems) was superimposed on the EGF–EGFR complex from the crystal structure (1NQL.pdb), as shown in Fig. 6. It is clearly seen that only the EGF/60CS/SWCNT/Gemzar DDS was able to bind with EGFR. Since the EGF conformation in this system was well aligned to the crystal EGF while the rest components of the DDS model were positioned outside the protein–protein binding region (Fig. 6b). In contrast, steric hindrance and bad contact were found between the SWCNT transporter of the EGF/30CS/SWCNT/Gemzar DDS and the EGFR (Fig. 6a). It is worth noting that in the initial structure there were 10 free chitosan units outside the SWCNT surface to prevent such steric hindrance (Fig. 2a). In order to avoid this prevention of the correct EGF–EGFR binding (on cancer cells), the ratio of chitosan MW per SWCNT surface area should be larger than 9.9×10^{-7} kg/m^2, based upon the MW of 50 units of single layer chitosan per outer surface area of SWCNT with 14 Å in diameter and 34 Å in length in the present study. The rational for using 50 chitosan units instead of 60 units as the minimum size is that 50 units of chitosan was long enough to wrap over the SWCNT surface in the EGF/60CS/SWCNT/Gemzar DDS while the remaining 10 chitosan units were located freely outside the SWCNT surface.

The temperature dependence of EGF localization from simulations with ff96/igb1, ff96/igb5 and ff03/igb5 were investigated by a plot of d[Cg(EGF) – Cg(CNT)] versus temperature (Fig. 7a–c). It can be observed that three different simulations likely provided the similar plot. EGF in both systems moved away from the SWCNT (from 20 to 48 Å in 30CS, and from 57 to 88 Å in 60CS) when the temperature increases from 300 to 455 K.

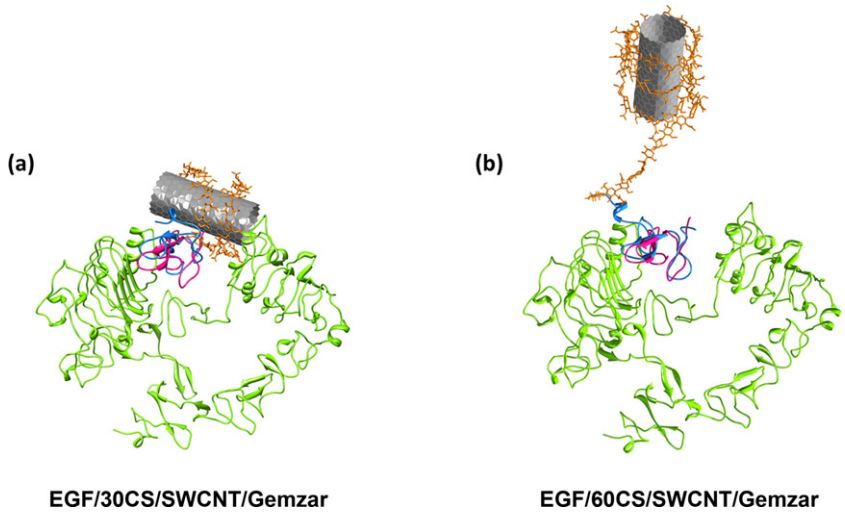

Fig. 6. Superimposition on the EGF structures between the global minimum (blue) of (a) the EGF/30CS/SWCNT/Gemzar and (b) EGF/60CS/SWCNT/Gemzar DDSs and the co-crystal structure of EGF (pink)-EGFR (green). (For interpretation of the references to color in this figure legend, the reader is referred to the web version of the article.)

3.3. Chitosan

At the initial state of the two DDS models (Fig. 2), only the first 10 chitosan units were freely located outside the length of the SWCNT, while the other 20 and 50 units in the EGF/30CS/SWCNT/Gemzar and EGF/60CS/SWCNT/Gemzar DDSs, respectively, were enfolded in a spiral orientation around the SWCNT outer surface. After REMD simulations, those first 10 chitosan units in the EGF/30CS/SWCNT/Gemzar system at 300 K move to enfolding around SWCNT making all 30 units of chitosan completely wrapped over SWCNT surface. In contrast with the EGF/60CS/SWCNT/Gemzar DDS, the first 10 chitosan units still locate outside SWCNT surface while other 50 chitosan units, from 11th to 60th terminal numbering in the EGF/60CS/SWCNT/Gemzar DDS completely wrapped around the SWCNT, as shown in the schematic view of Fig. 4. With the simulation result at 300 K as a reference, only the positions of chitosan units enfolded around the SWCNT, 11th to 60th chitosan units, were selected to evaluate the effect of temperatures to the enfolding of chitosan chain in EGF/60CS/SWCNT/Gemzar DDS.

To evaluate the chitosan spiral enfolding over SWCNT surface, the average distance from the centers of gravity of the wrapped chitosan units in a radial direction to the SWCNT curvature, d[Cg(^{wrap}CS) – ^{surface}CNT] were calculated. In all simulations (Fig. 8a1–c1), this focused distance versus temperature slightly increased where its slope from the fitted linear equation was in range of 0.002–0.004. This indicates that helical chitosan chain was less tightly wrapped on the tube surface at higher temperature. Additionally, the higher d[Cg(^{wrap}CS) – ^{surface}CNT] from simulation with 60CS (gray in Fig. 8a1–c1) by c.a. 0.5 Å denoted the enfolding of chitosan chain was less tightly in radial direction due to steric hindrance from fully wrapped units over the tube.

For enfolding of chitosan along the SWCNT length, the end-to-end distance of the wrapped units, d_z[Cg(^{1st}CS) – Cg(^{30th}CS)] or d_z[Cg(^{11th}CS) – Cg(^{60th}CS)] calculated in the direction parallel to the tube length (z direction), was plotted and compared in Fig. 8a2–c2. In all different simulations, the higher value of d_z[Cg(^{11th}CS) – Cg(^{60th}CS)] over d_z[Cg(^{1st}CS) – Cg(^{30th}CS)], shown as gray and black lines, was resulted from the longer wrapped chitosan units (50 units) around the tube in the 60CS system. As increase in temperature, all the end-to-end distances from the two simulations with igb5 solvation model (Fig. 8b2 and c2) expanded in range of 12.7–23.8 Å and 19.0–38.8 Å for systems with 30CS and 60CS, respectively. This is different for that of igb1 simulation (Fig. 8a2) which was not significantly raised up but fluctuated around 18.7–20.7 and 29.1 to 31.7 Å, respectively as can be seen from the slopes of fitting linear equation (0.004 and 0.017).

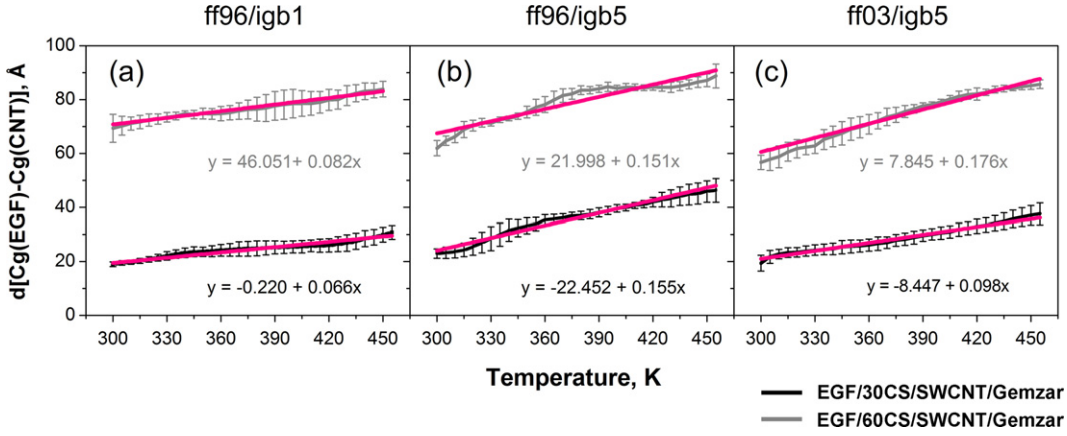

Fig. 7. The temperature dependence of the averaged distances between the center of gravity of EGF and SWCNT for the EGF/30CS/SWCNT/Gemzar DDS (black) and the EGF/60CS/SWCNT/Gemzar DDS (gray) with fitted liner equations (pink). The standard deviations are shown as vertical bars. (For interpretation of the references to color in this figure legend, the reader is referred to the web version of the article.)

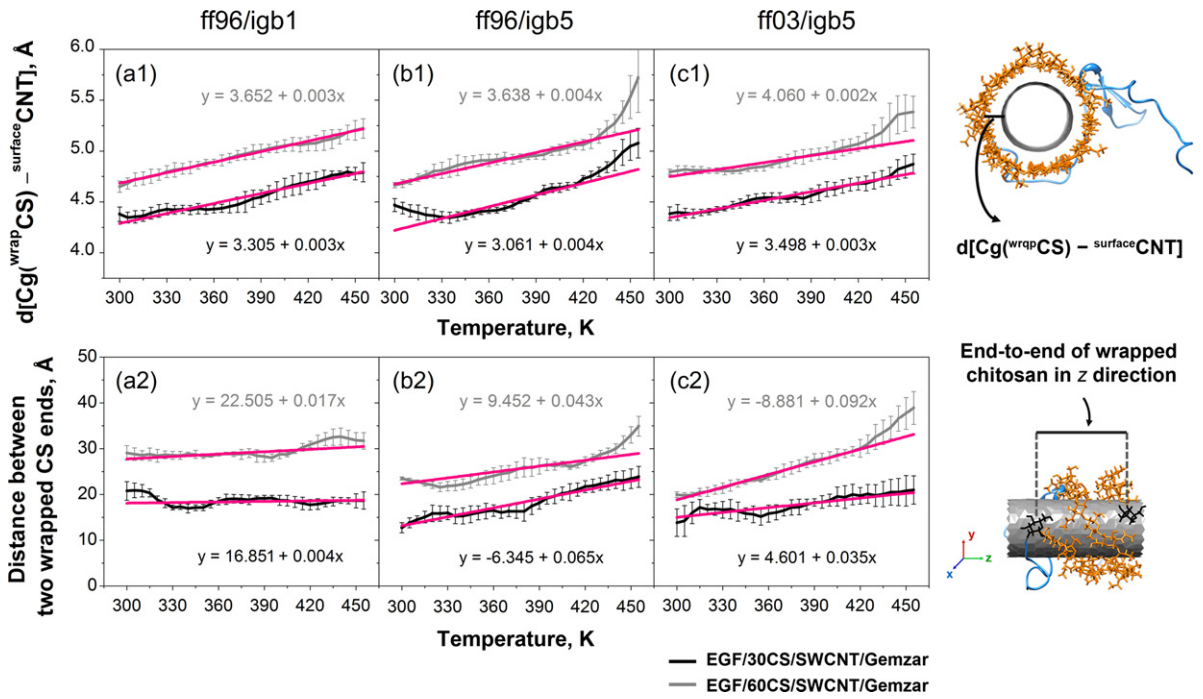

Fig. 8. Temperature dependence of (a1–c1) the averaged distance between the center of gravities of all chitosan units and the SWCNT surface, d[Cg(^{wrap}CS) – ^{surface}CNT], and (a2–c2) the average distance between two wrapped chitosan ends in the parallel direction to the SWCNT length or z direction which is d_z[Cg(^{1st}CS) – Cg(^{30th}CS)] for EGF/30CS/SWCNT/Gemzar (black) and d_z[Cg(^{11th}CS) – Cg(^{60th}CS)] for EGF/60CS/SWCNT/Gemzar DDSs (gray). The standard deviations are shown as vertical bars while fitted linear equations are shown in pink lines. (For interpretation of the references to color in this figure legend, the reader is referred to the web version of the article.)

Taken together, as temperature increases, chitosan chain can expand its structure either radial direction to the tube curvature or parallel direction to the tube length. Besides, the solvation model applied in the simulation showed an influence to the temperature dependent-chitosan enfolding especially in direction parallel to the tube length.

4. Gemcitabine drug

The displacement of gemcitabine inside the SWCNT cavity at different temperatures for the two systems was explored in terms of the distance between the center of gravity of gemcitabine and the SWCNT surface, d[Cg(drug) – ^{surface}CNT]. From the REMD simulations, the gemcitabine was always located inside the SWCNT cavity at all temperatures evaluated with distances from the SWCNT inner surface of 4.37–4.48 Å for both DDSs, even though the force field and solvation model applied were different, as shown in Fig. 9. Note that the plots of the distance versus temperature of two systems from the simulations with ff03/igb5 and ff96/igb5 (Fig. 9b and c) are nearly equal while more fluctuation was found in the rest calculation (Fig. 9a). In addition, the average d[Cg(drug) – ^{surface}CNT] values and slopes from fitted linear equations of EGF/30CS/SWCNT/Gemzar and EGF/60CS/SWCNT/Gemzar DDSs were almost equivalent, suggesting that the length of the wrapped chitosan chain outside of the SWCNT surface did not affect the movement of gemcitabine inside the cavity.

The obtained d[Cg(drug) – ^{surface}CNT] in this REMD study (Fig. 9) were slightly less than that of the previous classical MD study with explicit salvation model on a gemcitabine molecule inside pristine SWCNT (4.7 Å) [74] suggesting the partial π–π interaction between the cytosine ring of gemcitabine and the surface of the SWCNT. However, this interaction was considerably decreased by increase

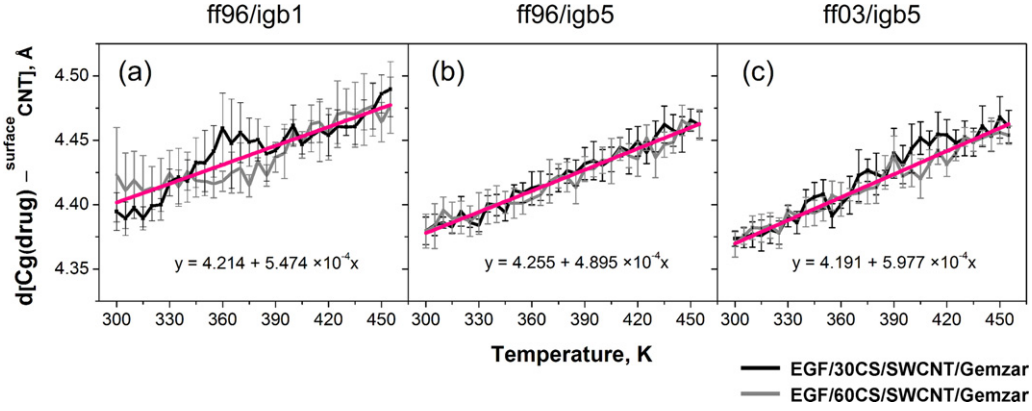

Fig. 9. Temperature dependence of the distance between the center of gravity of gemcitabine and the SWCNT surface, d[Cg(drug) – ^{surface}CNT], for the EGF/30CS/SWCNT/Gemzar (black) and EGF/60CS/SWCNT/Gemzar (gray) DDSs of the three sets of AMBER force fields and solvation models. The standard deviations are shown as vertical bars while fitted linear equations are shown in pink lines. (For interpretation of the references to color in this figure legend, the reader is referred to the web version of the article.)

in gemcitabine concentration loaded in the tube [77] implying that drugs easier release than a single encapsulated drug and may be released together from inside the tube cavity.

5. Conclusion

In this study, REMD simulations at temperatures ranging from 300 to 455 K with three different pairs of force fields and solvation models (ff96/igb1, ff96/igb5 and ff03/igb5) were performed on the EGF/30CS/SWCNT/Gemzar and EGF/60CS/SWCNT/Gemzar DDS models that vary in the size of the chitosan chain (30 or 60 units length), with the aim of exploring their molecular properties and dynamic behaviors at various temperatures. The distance to the tube center showed that EGF in both DDSs become transformed and moved away from the SWCNT drug transporter at high temperatures. The packing of the chitosan orbit around the SWCNT in the EGF/30CS/SWCNT/Gemzar DDS enforced the EGF to relocate nearby the tube surface and the secondary structure of EGF was deformed. Therefore the steric hindrance induced by chitosan and the SWCNT as well as secondary structure deformation may block the binding of EGF onto the EGFR. To avoid this possible phenomenon, the chitosan chain wrapped around the SWCNT should be long enough to cover the entire SWCNT surface, which was calculated to require a mininum ratio of chitosan MW per SWCNT surface area of 9.9×10^{-7} kg/m^2. Besides, the gemcitabine always stayed inside SWCNT at all simulation times with similar distances for possible π–π stacking formation toward the inner surface of SWCNT. The two DDS models provided the same temperature dependence in which the EGF structure was considerably unfolded and the chitosan chain was less packed around the tube, but the magnitude of temperature responses were differed, especially the results from simulation with ff96/igb1. Even though the results from REMD simulations with different of force fields and solvation models were not exactly similar but all of them suggested that EGF/60CS/SWCNT/Gemzar DDS was a good candidate for efficient targeted DDS. Taken altogether, the obtained data from this study provides useful information toward the design of an effective DDS in the future.

Acknowledgments

This work was supported by the Chulalongkorn University Centenary Academic Development Project (Under the Center of Innovative Nanotechnology, Chulalongkorn University), and the Higher Education Research Promotion and National Research University Project of Thailand, Office of the Higher Education Commission (HR1155A). The Thai Government Stimulus Package 2 (TKK2555) under the Project for Establishment of Comprehensive Center for Innovative Food, Health Products and Agriculture is greatly acknowledged for computing resources. C.R. thanks the Royal Golden Jubilee Ph.D. Program (PHD/0325/2551) for financial support. Finally, the authors would like to give special acknowledgment to the JENESYS Program 2011 under JSPS exchange program for East Asian young researchers for offering the research collaboration opportunity between Japan and Thailand.

References

[1] S. Iijima, Helical microtubules of graphitic carbon, Nature 354 (1991) 56–58.
[2] W.R. Yang, P. Thordarson, J.J. Gooding, S.P. Ringer, F. Braet, Carbon nanotubes for biological and biomedical applications, Nanotechnology 18 (2007) 12.
[3] D. Tasis, N. Tagmatarchis, A. Bianco, M. Prato, Chemistry of carbon nanotubes, Chemical Reviews 106 (2006) 1105–1136.
[4] A. Bianco, K. Kostarelos, M. Prato, Applications of carbon nanotubes in drug delivery, Current Opinion in Chemical Biology 9 (2005) 674–679.
[5] G. Pastorin, Crucial functionalizations of carbon nanotubes for improved drug delivery: a valuable option, Pharmaceutical Research 26 (2009) 746–769.
[6] B.I. Kharisov, O.V. Kharissova, H.L. Gutierrez, U.O. Mendez, Recent advances on the soluble carbon nanotubes, Industrial and Engineering Chemistry Research 48 (2009) 572–590.
[7] C. Iamsamai, S. Hannongbua, U. Ruktanonchai, A. Soottitantawat, S.T. Dubas, The effect of the degree of deacetylation of chitosan on its dispersion of carbon nanotubes, Carbon 48 (2010) 25–30.
[8] Y.-L. Zhao, J.F. Stoddart, Noncovalent functionalization of single-walled carbon nanotubes, Accounts of Chemical Research 42 (2009) 1161–1171.
[9] C. Chen, X.-X. Xie, Q. Zhou, F.-Y. Zhang, Q.-L. Wang, Y.-Q. Liu, Y. Zou, Q. Tao, X.-M. Ji, S.-Q. Yu, EGF-functionalized single-walled carbon nanotubes for targeting delivery of etoposide, Nanotechnology 23 (2012) 045104.
[10] T. Rungrotmongkol, U. Arsawang, C. Iamsamai, A. Vongachariya, S.T. Dubas, U. Ruktanonchai, A. Soottitantawat, S. Hannongbua, Increased dispersion and solubility of carbon nanotubes noncovalently modified by the polysaccharide biopolymer, chitosan: MD simulations, Chemical Physics Letters 507 (2011) 134–137.
[11] X.K. Zhang, L.J. Meng, Q.G. Lu, Z.F. Fei, P.J. Dyson, Targeted delivery and controlled release of doxorubicin to cancer cells using modified single wall carbon nanotubes, Biomaterials 30 (2009) 6041–6047.
[12] J.H. Park, G. Saravanakumar, K. Kim, I.C. Kwon, Targeted delivery of low molecular drugs using chitosan and its derivatives, Advanced Drug Delivery Reviews 62 (2010) 28–41.
[13] A. Galbiati, C. Tabolacci, B.M. Della Rocca, P. Mattioli, S. Beninati, G. Paradossi, A. Desideri, Targeting tumor cells through chitosan–folate modified microcapsules loaded with camptothecin, Bioconjugate Chemistry 22 (2011) 1066–1072.
[14] S.K. Sahu, S. Maiti, T.K. Maiti, S.K. Ghosh, P. Pramanik, Hydrophobically modified carboxymethyl chitosan nanoparticles targeted delivery of paclitaxel, Journal of Drug Targeting 19 (2011) 104–113.
[15] D. Depan, J. Shah, R.D.K. Misra, Controlled release of drug from folate-decorated and graphene mediated drug delivery system: synthesis, loading efficiency, and drug release response, Materials Science and Engineering: C 31 (2011) 1305–1312.
[16] http://www.who.int/en/
[17] D.K. Kim, J. Dobson, Nanomedicine for targeted drug delivery, Journal of Materials Chemistry 19 (2009) 6294–6307.
[18] J. Chen, S. Chen, X. Zhao, L.V. Kuznetsova, S.S. Wong, I. Ojima, Functionalized single-walled carbon nanotubes as rationally designed vehicles for tumor-targeted drug delivery, Journal of the American Chemical Society 130 (2008) 16778–16785.
[19] N. Normanno, A. De Luca, C. Bianco, L. Strizzi, M. Mancino, M.R. Maiello, A. Carotenuto, G. De Feo, F. Caponigro, D.S. Salomon, Epidermal growth factor receptor (EGFR) signaling in cancer, Gene 366 (2006) 2–16.
[20] J.S. Nielsen, E. Jakobsen, B. HØlund, K. Bertelsen, A. Jakobsen, Prognostic significance of p53, Her-2, and EGFR overexpression in borderline and epithelial ovarian cancer, International Journal of Gynecological Cancer 14 (2004) 1086–1096.
[21] L.C. Hartmann, G.L. Keeney, W.L. Lingle, T.J.H. Christianson, B. Varghese, D. Hillman, A.L. Oberg, P.S. Low, Folate receptor overexpression is associated with poor outcome in breast cancer, International Journal of Cancer 121 (2007) 938–942.
[22] S. Acharya, F. Dilnawaz, S.K. Sahoo, Targeted epidermal growth factor receptor nanoparticle bioconjugates for breast cancer therapy, Biomaterials 30 (2009) 5737–5750.
[23] C.L. Tseng, S.Y.H. Wu, W.H. Wang, C.L. Peng, F.H. Lin, C.C. Lin, T.H. Young, M.J. Shieh, Targeting efficiency and biodistribution of biotinylated-EGF-conjugated gelatin nanoparticles administered via aerosol delivery in nude mice with lung cancer, Biomaterials 29 (2008) 3014–3022.
[24] L.L. Yang, H. Mao, Y.A. Wang, Z.H. Cao, X.H. Peng, X.X. Wang, H.W. Duan, C.C. Ni, Q.G. Yuan, G. Adams, M.Q. Smith, W.C. Wood, X.H. Gao, S.M. Nie, Single chain epidermal growth factor receptor antibody conjugated nanoparticles for in vivo tumor targeting and imaging, Small 5 (2009) 235–243.
[25] J. Mendelsohn, The epidermal growth factor receptor as a target for cancer therapy, Endocrine-Related Cancer 8 (2001) 3–9.
[26] D.J. Leahy, Structure and function of the epidermal growth factor (EGF/ErbB) family of receptors, Advances in Protein Chemistry 68 (2004) 1–27.
[27] H. Ogiso, R. Ishitani, O. Nureki, S. Fukai, M. Yamanaka, J.-H. Kim, K. Saito, A. Sakamoto, M. Inoue, M. Shirouzu, S. Yokoyama, Crystal structure of the complex of human epidermal growth factor and receptor extracellular domains, Cell 110 (2002) 775–787.
[28] A. Richter, D.R. Drummond, J. MacGarvie, S.M. Puddicombe, S.G. Chamberlin, D.E. Davies, Contribution of the transforming growth factor B-loop-sheet to binding and activation of the epidermal growth factor receptor, Journal of Biological Chemistry 270 (1995) 1612–1616.
[29] M.A. Lemmon, Ligand-induced ErbB receptor dimerization, Experimental Cell Research 315 (2009) 638–648.
[30] J.P. Dawson, Z. Bu, M.A. Lemmon, Ligand-induced structural transitions in ErbB receptor extracellular domains, Structure 15 (2007) 942–954.
[31] K.M. Ferguson, M.B. Berger, J.M. Mendrola, H.-S. Cho, D.J. Leahy, M.A. Lemmon, EGF activates its receptor by removing interactions that autoinhibit ectodomain dimerization, Molecular Cell 11 (2003) 507–517.
[32] G. Lurje, H.J. Lenz, EGFR signaling and drug discovery, Oncology 77 (2009) 400–410.
[33] S. Yano, K. Kondo, M. Yamaguchi, G. Richmond, M. Hutchison, A. Wakeling, S. Averbuch, P. Wadsworth, Distribution and function of EGFR in human tissue

and the effect of EGFR tyrosine kinase inhibition, Anticancer Research 23 (2003) 3639–3650.
[34] T. Mitsudomi, Advances in target therapy for lung cancer, Japanese Journal of Clinical Oncology 40 (2010) 101–106.
[35] R.S. Herbst, P.A. Bunn, Targeting the epidermal growth factor receptor in non-small cell lung cancer, Clinical Cancer Research 9 (2003) 5813–5824.
[36] B. Corkery, J. Crown, M. Clynes, N. O'Donovan, Epidermal growth factor receptor as a potential therapeutic target in triple-negative breast cancer, Annals of Oncology 20 (2009) 862–867.
[37] R.I. Nicholson, J.M.W. Gee, M.E. Harper, EGFR and cancer prognosis, European Journal of Cancer 37 (2001) 9–15.
[38] A.A. Bhirde, V. Patel, J. Gavard, G.F. Zhang, A.A. Sousa, A. Masedunskas, R.D. Leapman, R. Weigert, J.S. Gutkind, J.F. Rusling, Targeted killing of cancer cells in vivo and in vitro with EGF-directed carbon nanotube-based drug delivery, ACS Nano 3 (2009) 307–316.
[39] J.G. Ji, D.J. Wu, L. Liu, J.D. Chen, Y. Xu, Preparation, characterization, and in vitro release of folic acid-conjugated chitosan nanoparticles loaded with methotrexate for targeted delivery, Polymer Bulletin 68 (2012) 1707–1720.
[40] V.V. Chaban, T.I. Savchenko, S.M. Kovalenko, O.V. Prezhdo, Heat-driven release of a drug molecule from carbon nanotubes: a molecular dynamics study, Journal of Physical Chemistry B 114 (2010) 13481–13486.
[41] P. Chakravarty, R. Marches, N.S. Zimmerman, A.D.E. Swafford, P. Bajaj, I.H. Musselman, P. Pantano, R.K. Draper, E.S. Vitetta, Thermal ablation of tumor cells with anti body-functionalized single-walled carbon nanotubes, Proceedings of the National Academic Sciences 105 (2008) 8697–8702.
[42] T. Rungrotmongkol, T. Udommaneethanakit, M. Malaisree, N. Nunthaboot, P. Intharathep, P. Sompornpisut, S. Hannongbua, How does each substituent functional group of oseltamivir lose its activity against virulent H5N1 influenza mutants, Biophysical Chemistry 145 (2009) 29–36.
[43] A. Tongraar, T. Kerdcharoen, S. Hannongbua, Simulations of liquid ammonia based on the combined quantum mechanical/molecular mechanical (QM/MM) approach, Journal of Physical Chemistry A 110 (2006) 4924–4929.
[44] M. Malaisree, T. Rungrotmongkol, N. Nunthaboot, O. Aruksakunwong, P. Intharathep, P. Decha, P. Sompornpisut, S. Hannongbua, Source of oseltamivir resistance in avian influenza H5N1 virus with the H274Y mutation, Amino Acids 37 (2009) 725–732.
[45] M. Kiselev, S. Noskov, Y. Puhovski, T. Kerdcharoen, S. Hannongbua, The study of hydrophobic hydration in supercritical water–methanol mixtures, Journal of Molecular Graphics and Modelling 19 (2001) 412–416.
[46] C. Laohpongspaisan, T. Rungrotmongkol, P. Intharathep, M. Malaisree, P. Decha, O. Aruksakunwong, P. Sompornpisut, S. Hannongbua, Why amantadine loses its function in influenza M2 mutants: MD simulations, Journal of Chemical Information and Modeling 49 (2009) 847–852.
[47] X. Yongqiang, C. Maodu, Dynamics of molecules translocating through carbon nanotubes as nanofluidic channels, Nanotechnology 17 (2006) 5216.
[48] I.-C. Yeh, G. Hummer, Nucleic acid transport through carbon nanotube membranes, Proceedings of the National Academic Sciences 101 (2004) 12177–12182.
[49] P. Sornmee, T. Rungrotmongkol, O. Saengsawang, U. Arsawang, T. Remsungnen, S. Hannongbua, Understanding the molecular properties of doxorubicin filling inside, and wrapping outside, single-walled carbon nanotubes, J. Comput. Theor. Nanos. 8 (2011) 1385–1391.
[50] Y. Sugita, Y. Okamoto, Replica-exchange molecular dynamics method for protein folding, Chemical Physics Letters 314 (1999) 141–151.
[51] K. Hukushima, K. Nemoto, Exchange Monte Carlo method and application to spin glass simulations, Journal of the Physical Society of Japan 65 (1996) 1604–1608.
[52] A. Mitsutake, Y. Sugita, Y. Okamoto, Generalized-ensemble algorithms for molecular simulations of biopolymers, Peptide Science 60 (2001) 96–123.
[53] H. Nymeyer, S. Gnanakaran, A.E. García, Atomic simulations of protein folding, using the replica exchange algorithm, Methods in Enzymology 383 (2004) 119–149.
[54] X. Cheng, G. Cui, V. Hornak, C. Simmerling, Modified replica exchange simulation methods for local structure refinement, Journal of Physical Chemistry B 109 (2005) 8220–8230.
[55] U.H.E. Hansmann, Parallel tempering algorithm for conformational studies of biological molecules, Chemical Physics Letters 281 (1997) 140–150.
[56] C. Yan, V. Pattani, J.W. Tunnell, P. Ren, Temperature-induced unfolding of epidermal growth factor (EGF): insight from molecular dynamics simulation, Journal of Molecular Graphics and Modelling 29 (2010) 2–12.
[57] R.R. Johnson, A. Kohlmeyer, A.T.C. Johnson, M.L. Klein, Free energy landscape of a DNA–carbon nanotube hybrid using replica exchange molecular dynamics, Nano Letters 9 (2009) 537–541.
[58] A. Suenaga, Replica-exchange molecular dynamics simulations for a small-sized protein folding with implicit solvent, Journal of Molecular Structure: THEOCHEM 634 (2003) 235–241.
[59] S.G. Itoh, H. Okumura, Y. Okamoto, Replica-exchange method in van der Waals radius space: overcoming steric restrictions for biomolecules, Journal of Chemical Physics 132 (2010) 134105.
[60] P. Kar, W. Nadler, U.H.E. Hansmann, Microcanonical replica exchange molecular dynamics simulation of proteins, Physical Review E 80 (2009) 056703.
[61] M. Kouza, U.H.E. Hansmann, Velocity scaling for optimizing replica exchange molecular dynamics, Journal of Chemical Physics 134 (2011), 044124-6.
[62] P. Ferrara, J. Apostolakis, A. Caflisch, Evaluation of a fast implicit solvent model for molecular dynamics simulations, Proteins: Structure, Function, and Bioinformatics 46 (2002) 24–33.
[63] W.C. Still, A. Tempczyk, R.C. Hawley, T. Hendrickson, Semianalytical treatment of solvation for molecular mechanics and dynamics, Journal of the American Chemical Society 112 (1990) 6127–6129.
[64] M.S. Shell, R. Ritterson, K.A. Dill, A test on peptide stability of AMBER force fields with implicit solvation, The Journal of Physical Chemistry B 112 (2008) 6878–6886.
[65] G.D. Hawkins, C.J. Cramer, D.G. Truhlar, Parametrized models of aqueous free energies of solvation based on pairwise descreening of solute atomic charges from a dielectric medium, The Journal of Physical Chemistry 100 (1996) 19824–19839.
[66] A. Onufriev, D. Bashford, D.A. Case, Exploring protein native states and large-scale conformational changes with a modified generalized born model, Proteins: Structure, Function, and Bioinformatics 55 (2004) 383–394.
[67] M. Feig, A. Onufriev, M.S. Lee, W. Im, D.A. Case, C.L. Brooks, Performance comparison of generalized born and Poisson methods in the calculation of electrostatic solvation energies for protein structures, Journal of Computational Chemistry 25 (2004) 265–284.
[68] J. Mongan, C. Simmerling, J.A. McCammon, D.A. Case, A. Onufriev, Generalized born model with a simple, robust molecular volume correction, Journal of Chemical Theory and Computation 3 (2006) 156–169.
[69] E. Sabini, S. Hazra, M. Konrad, A. Lavie, Nonenantioselectivity property of human deoxycytidine kinase explained by structures of the enzyme in complex with L- and D-nucleosides, Journal of Medicinal Chemistry 50 (2007) 3004–3014.
[70] A.M. Ferrari, G. Degliesposti, M. Sgobba, G. Rastelli, Validation of an automated procedure for the prediction of relative free energies of binding on a set of aldose reductase inhibitors, Bioorganic and Medicinal Chemistry 15 (2007) 7865–7877.
[71] X. Lu, Z. Chen, Curved pi-conjugation, aromaticity, and the related chemistry of small fullerenes (<C60) and single-walled carbon nanotubes, Chemical Reviews 105 (2005) 3643–3696.
[72] Y. Duan, C. Wu, S. Chowdhury, M.C. Lee, G. Xiong, W. Zhang, R. Yang, P. Cieplak, R. Luo, T. Lee, J. Caldwell, J. Wang, P. Kollman, A point-charge force field for molecular mechanics simulations of proteins based on condensed-phase quantum mechanical calculations, Journal of Computational Chemistry 24 (2003) 1999–2012.
[73] M.B. Tessier, M.L. DeMarco, A.B. Yongye, R.J. Woods, Extension of the GLYCAM06 biomolecular force field to lipids, lipid bilayers and glycolipids, Molecular Simulation 34 (2008) 349–364.
[74] U. Arsawang, O. Saengsawang, T. Rungrotmongkol, P. Sornmee, K. Wittayanarakul, T. Remsungnen, S. Hannongbua, How do carbon nanotubes serve as carriers for gemcitabine transport in a drug delivery system? Journal of Molecular Graphics and Modelling 29 (2011) 591–596.
[75] D. Boldor, N.M. Gerbo, W.T. Monroe, J.H. Palmer, Z. Li, A.S. Biris, Temperature measurement of carbon nanotubes using infrared thermography, Chemistry of Materials 20 (2008) 4011–4016.
[76] W. Kabsch, C. Sander, Dictionary of protein secondary structure: pattern recognition of hydrogen-bonded and geometrical features, Biopolymers 22 (1983) 2577–2637.
[77] C. Rungnim, U. Arsawang, T. Rungrotmongkol, S. Hannongbua, Molecular dynamics properties of varying amounts of the anticancer drug gemcitabine inside an open-ended single-walled carbon nanotube, Chemical Physics Letters 550 (2012) 99–103.